Nuclear Analyses for the Assessment of the Loads on the ITER Radial Neutron Camera In-Port System and Evaluation of Its Measurement Performances

Fabio Moro, Daniele Marocco, Francesco Belli, Giorgio Brolatti, Andrea Colangeli, Fabio Crescenzi, Davide Flammini, Nicola Fonnesu, Giada Gandolfo, Ryszard Kantor, Giovanni Mariano, Domenico Marzullo, Salvatore Podda, Dustin Sancristóbal, Rosaria Villari, and Basilio Esposito

***Abstract*— The radial neutron camera (RNC) is a key ITER diagnostic system designed to measure the uncollided 14- and 2.5-MeV neutrons from deuterium–tritium (DT) and deuterium–deuterium (DD) fusion reactions, through an array of detectors covering a full poloidal plasma section along collimated lines of sight (LoS). Its main objective is the assessment of the neutron emissivity/α source profile and the total neutron source strength, providing spatially resolved measurements of several parameters needed for fusion power estimation, plasma control, and plasma physics studies. The present RNC layout is composed of two fan-shaped collimating structures viewing the plasma radially through vertical slots in the diagnostic shielding module (DSM) of ITER Equatorial Port 1 (EP01): the ex-port subsystem and the in-port one. The ex-port subsystem, devoted to the plasma core coverage, extends from the Port Interspace to the Bioshield Plug: it consists of a massive shielding unit hosting two sets of collimators lying on different toroidal planes, leading to a total of 16 interleaved LoS. The in-port system consists of a cassette, integrated inside the port plug DSM, containing two detectors per each of the six LoS looking at the plasma edges. The in-port system must guarantee the required measurement performances in critical operating conditions in terms of high radiation levels, given its proximity to the plasma neutron source. This article presents an updated neutronic analysis based on the latest design of the in-port system and port plug. It has been performed by means of the Monte Carlo MCNP code and provides nuclear loads on the in-port RNC during normal operating conditions (NOC) and inputs for the measurement performance analysis.**

***Index Terms*— ITER, MCNP, Monte Carlo methods, neutron diagnostics, neutron measurements, radial neutron camera (RNC), radiation transport.**

I. Introduction

THE radial neutron camera (RNC) is a diagnostic system located in the ITER Equatorial Port #1 (EP01) whose main function is the measurement of uncollided 14- and 2.5-MeV neutrons from deuterium–tritium (DT) and deuterium–deuterium (DD) fusion reactions through an array of flux monitors/spectrometers located in collimated lines of sight (LoS). The line-integrated neutron fluxes are used to assess the local radial profile of plasma neutrons emitted per unit time and volume (neutron emissivity [1], [2]) and, therefore, the neutron yield and the alpha particles' birth profile. The temperature profile of the bulk ions can be derived [3] from the Doppler broadened widths of the RNC line-integrated spectra that also provide insights into the supra-thermal ions produced by the injection in the plasma of electromagnetic waves and neutral particles. Moreover, the RNC emissivity and temperature measurements can be employed to estimate the composition of the ITER fuel, namely the ratio between the tritium and deuterium densities [1].

The RNC (Fig. 1) is based on two fan-shaped collimating structures viewing the plasma radially through optical paths in the EP01 diagnostic first wall (DFW) and diagnostic shielding module (DSM) [4], [5]. The DFW and DSM, whose role is the protection of the diagnostics from the plasma heat loads and provide adequate nuclear shielding for port cells, vacuum vessels, and magnets are shown in Fig. 5 (right panel).

The ex-port RNC, devoted to probe the plasma core coverage ($r/a < 0.54$, a = minor radius), consists of a massive

Manuscript received 13 February 2022; revised 5 May 2022; accepted 6 June 2022. This work was supported in part by CRESCO/ENEAGRID High Performance Computing Infrastructure which is funded by ENEA, the Italian National Agency for New Technologies, Energy and Sustainable Economic Development, and the Italian and European Research Programmes (see http://www.cresco.enea.it/english) and in part by Fusion for Energy under Agreement F4E-FPA-327 (Specific Contracts 06 and 07). The review of this article was arranged by Senior Editor G. H. Neilson. *(Corresponding author: Fabio Moro.)*

Fabio Moro, Daniele Marocco, Francesco Belli, Giorgio Brolatti, Andrea Colangeli, Fabio Crescenzi, Davide Flammini, Nicola Fonnesu, Giada Gandolfo, Giovanni Mariano, Salvatore Podda, Rosaria Villari, and Basilio Esposito are with ENEA, Department of Fusion and Nuclear Safety Technology, 00044 Frascati (Rome), Italy (e-mail: fabio.moro@enea.it).

Ryszard Kantor is with the Institute of Nuclear Physics, PAN, 31-342 Kraków, Poland.

Domenico Marzullo is with the Department of Engineering and Architecture, Trieste University, 34127 Trieste, Italy.

Dustin Sancristóbal is with IDOM s.a., 08940 Barcelona, Spain.

Color versions of one or more figures in this article are available at https://doi.org/10.1109/TPS.2022.3185801.

Digital Object Identifier 10.1109/TPS.2022.3185801

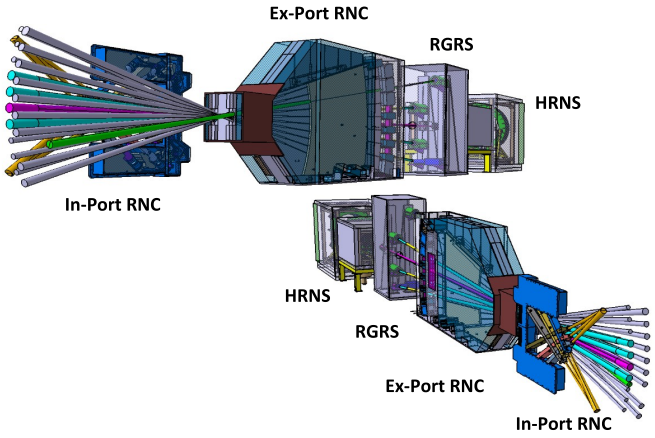

Fig. 1. Overall layout of RNC. Other interfacing diagnostics (RGRS and HRNS) are also indicated.

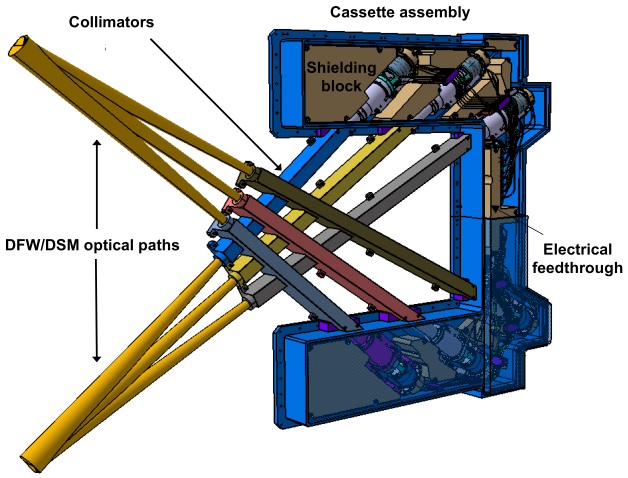

Fig. 2. In-port RNC subsystem.

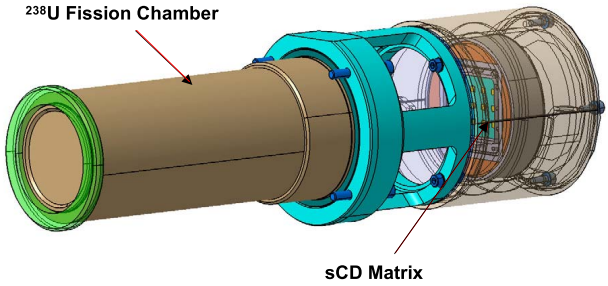

Fig. 3. In-port RNC detectors assembly.

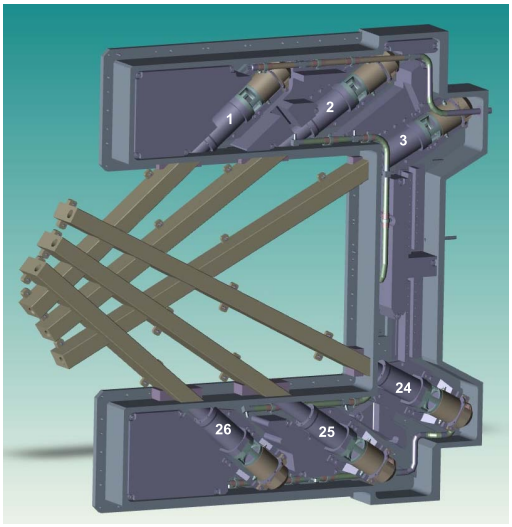

Fig. 4. In-port RNC MCNP model: 3-D representation showing the cassette inner structure (outer cassette wall removed), and the collimators assembly. LoS numbering is also reported.

shielding unit extending from the Port Interspace to the Bioshield Plug that hosts two sets of collimators lying on different toroidal planes, leading to a total of 16 interleaved LoS equipped with scintillators and diamond detectors. The four central collimators of the right set (looking toward the plasma) are, respectively, dedicated to the Radial Gamma Ray Spectrometer (RGRS, three LoS) and the High Resolution Neutron Spectrometer (HRNS, one LoS), both placed backward, in the Port Cell.

The in-port RNC (Fig. 2), integrated with the DSM Drawer #3 of the EP01, consists of a removable stainless steel cassette [SS316L(N)-IG], equipped with electrical and vacuum feedthrough, with two sets of three LoS each, looking at the plasma edges ($r/a > 0.67$).

The neutrons from the plasma are collected by means of conical optical paths hollowed out in the DFW and DSM and pass through the collimators up to the detector modules (Fig. 3) that contain two in-line devices: a single-crystal diamond (sCD) matrix as the main detector, also enabling spectrometric measurements [6], and a ^{238}U fission chamber (FC) as the complementary detector. The sCD is also complemented with specific α calibration sources (^{239}Pu, ^{241}Am, and ^{244}Cm [7]). The available space inside the cassette is filled with sintered boron carbide (B_4C) shielding blocks and beam dumps, in order to ensure a sufficient neutron streaming mitigation toward the Port Interspace area.

The in-port RNC has to withstand severe environmental conditions during ITER operations in terms of thermal, magnetic, and radiation fields. The present study aims at evaluating the nuclear loads and the neutron/gamma spectra at the detector's position for the in-port subsystem. Such analysis enables the optimization of the RNC design and provides data for thermo-mechanical studies and the assessment of the diagnostic measurement performances.

This article presents the nuclear analysis in the preparation for the final design review of the in-port RNC and updates the previous analysis [8].

II. In-Port RNC MCNP Model: Generation and Integration

A detailed MCNP [9] model of the in-port RNC has been developed through the conversion of a preprocessed engineering CAD model, by means of the SuperMC code [10] CAD-to-MCNP interface (Fig. 4). With respect to the previous layout [8], some important design changes have been implemented.

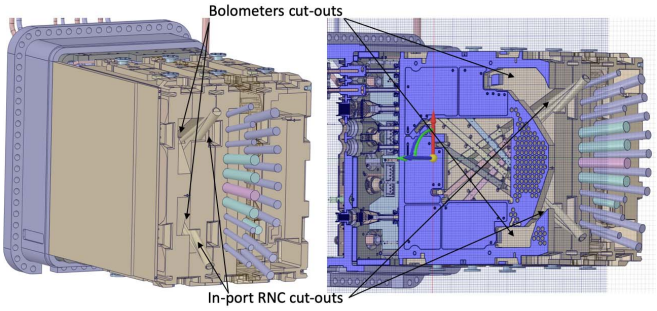

Fig. 5. EP01 layout: overall view showing the in-port RNC and Bolometer cut-outs (left panel) and section along the Bolometer cut-outs (right panel).

TABLE I
DIAGNOSTICS SYSTEM INTEGRATED IN THE EP01 DSM DRAWERS MCNP MODEL

DSM	Diagnostics
1	Divertor Impurity Monitor
	Motional Stark Effect based on heating beam
	Pressure Gauges
2	Radial Neutron Camera (ex-port subsystem)
	Radial Gamma Ray Spectrometers
	High Resolution Neutron Spectrometer
	Bolometers
3	Radial Neutron Camera (in-port subsystem)
	Neutron Flux Monitors
	Bolometers

1) Cassette thickness was reduced from 20 to 10 mm.
2) Reduced quantity of shielding material (B_4C, from 0.072 to 0.044 m^3) in order to allow the arrangement of other components.
3) Absence of the DSM shielding in the area where the collimators intersect.

The generated MCNP model of the in-port RNC has been successfully integrated into an upgraded version of the ITER C-model (release R181031 [11]), provided by the port integrator, in which the EP01 features are incorporated in the central equatorial port (Table I) including all the diagnostic systems and related cut-outs (e.g., bolometers penetrations, close to the in-port cassette and collimators, Fig. 5), so that crosstalk effects are taken into account. Such components were not included in the previous analysis [8], since their engineering design was at a preliminary stage of development.

The obtained geometry (Fig. 6) consists of a 40° regular sector of the tokamak representing all the components up to the Bioshield, where the EP01 structure is integrated into the central full-size equatorial port, while the half ports on the sides are filled with a diagnostic generic equatorial port plug (DGEPP), with dummy DFW and DSM [12]. The central upper and lower ports host a diagnostic upper equatorial Port Plug and a Torus Cryopump Lower Port, respectively. Periodic boundary conditions are toroidally applied at the planes that delimit the sector, in order to properly simulate the whole tokamak. The model also includes material specifications for particle transport, using the FENDL-3.1d [13] nuclear data libraries.

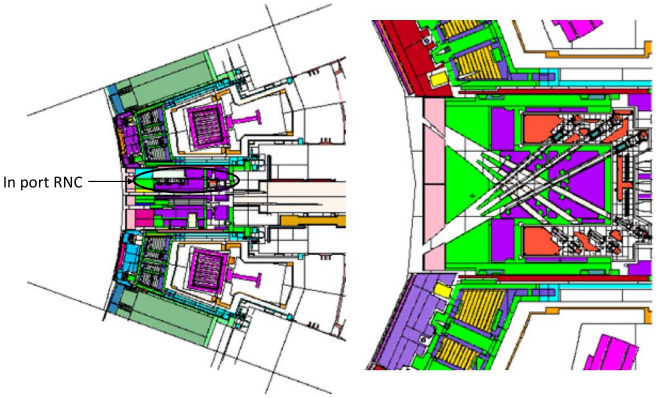

Fig. 6. ITER C-model integrating the EP01 features, with the in-port RNC structure in the full central equatorial port: toroidal section showing the positioning of the diagnostic assembly (left) and poloidal section across the upper collimators (right). The right panel highlights the positioning of the in-port RNC with respect to the DFW (pink area) and the port plug structure/DSM (green and violet cells, respectively).

The calculations for the evaluation of nuclear loads have been performed using the standard ITER plasma source provided with the C-model (inductive H-mode, 10 MA/5.3 T, 500-MW fusion power, and neutron rate: 1.773×10^{20} s^{-1}), while the assessment of the spectra at the detectors has been computed using a 15-MA peaked density DT neutron source (neutron rate: 1.83×10^{20} s^{-1}).

III. NUCLEAR LOADS ON THE IN-PORT RNC SUBCOMPONENTS

The following nuclear responses have been computed in 3-D maps format (1-cm voxel size), using the MCNP FMESH tally capability with proper tally multipliers which take into account materials, involving nuclear reactions and normalization factors:

1) neutron and gamma flux;
2) nuclear heating density;
3) damage and He production on stainless steel.

In order to achieve the statistical compliance on each mesh voxel (statistical uncertainty on each voxel $<10\%$ in the area of interest), variance reduction techniques have been used: specific mesh-based weigh-windows for neutrons and photons have been generated by means of the Advantg hybrid code [14] and successively customized in order to avoid excessive particles over-splitting in specific areas.

Sections of the total neutron flux map, along the upper and lower collimators axes, are provided in Fig. 7. It is ought to be highlighted that the mesh used does not extend up to the DFW, where the average neutron flux is around 2×10^{14} n/cm^2/s [15]. The neutron flux in the rear region of the cassette ($\sim 1.6 \times 10^{9}$ n/cm^2/s) is found to be lower by ~ 2 orders of magnitude than in the most exposed area of the cassette (closer to the DFW, $\sim 2 \times 10^{11}$ n/cm^2/s). The reduction in the neutron streaming is due to the B_4C high neutron capture cross section [through (n, γ) reactions]: this effect is clearly highlighted by the low flux spots inside the cassette body and along the collimating structures, beyond the detectors, where the beam dumps are installed. At the

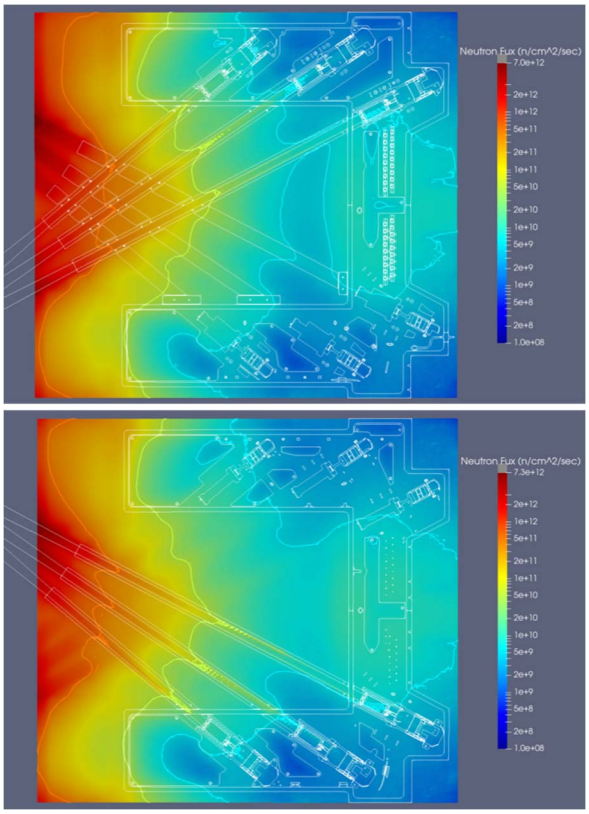

Fig. 7. Sections of the total neutron flux (n/cm^2/s) map across the upper LoS (top panel) and lower LoS (bottom panel).

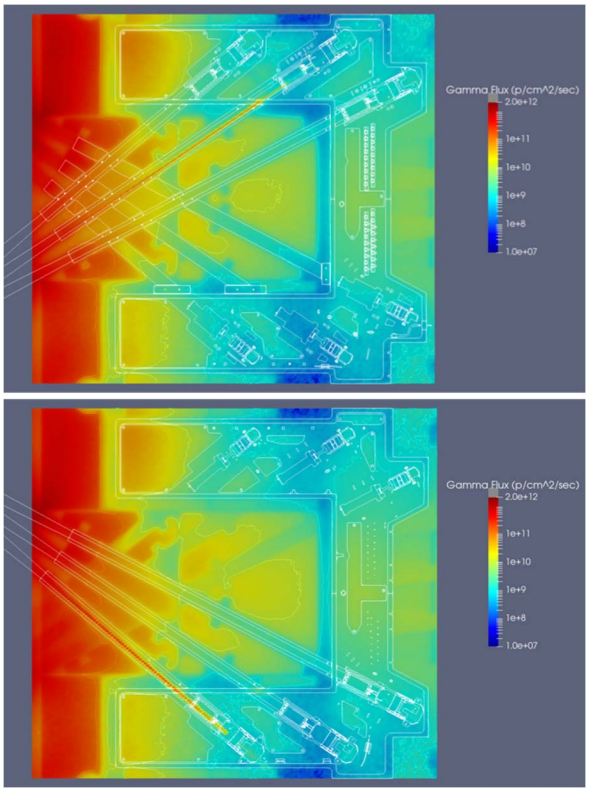

Fig. 8. Sections of the total gamma flux (γ/cm^2/s) map across the upper LoS (top panel) and lower LoS (bottom panel).

same time, an enhancement in the gamma flux is observed, especially in the front part of the cassette at the location of the B_4C slabs (Fig. 8). The consistent production of prompt photons generated in the area close to the detectors producing unwanted background on the sCD neutron signal is mitigated in the present design by the use of a 2.5-mm-thick plasma-sprayed tungsten layer deposited around the sCD detector housing.

The assessment of the nuclear heating density has been performed considering both the contribution of neutrons and secondary gammas. The heat load density spatial distribution shows a significant gradient (about four orders of magnitude) from the collimator openings toward the penetrations in the DSM ($\sim 10^{-2}$ W/cm^3) and back area of the cassette ($\sim 10^{-6}$ W/cm^3). The nuclear heating values for the various components of the in-port cassette (Fig. 9) are provided in Table II and have been used as input for the thermal and thermomechanical analyses [16].

The nuclear heating on the FC detectors ranges from a minimum of $\sim 1.3 \times 10^{-5}$ W/cm^3 (LoS 25) to a maximum of 8.6×10^{-5} W/cm^3 (LoS 1). Taking into account the nuclear heating and thermal loads due to direct contact and thermal radiation with the DSM, it is found (Fig. 10) that the maximum temperature reached by the detectors during NOC (normal operating conditions) is about 80 °C, which is well below the maximum acceptable temperature for proper functioning ($\leq$200 °C for the sCD and $\leq$260 °C for the FC).

The damage (dpa/fpy), assessed by means of the Norgett–Robinson–Torrens (NRT) model [17], and the He production

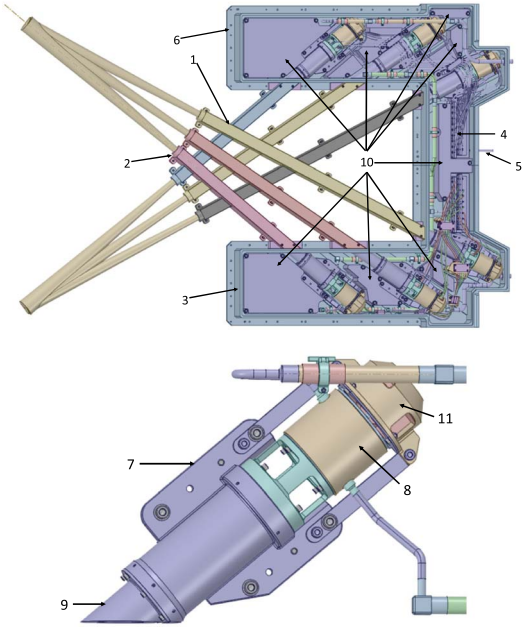

Fig. 9. Nuclear heating calculation: numbering of in-port cassette components (top) and detector module (bottom).

(appm/fpy) data both evaluated on stainless steel are reported in the 3-D maps in Fig. 11. The maximum values computed inside the collimator tubes in the area close to the in-port cutouts are $\sim$0.02 dpa/fpy for the damage and $\sim$0.1 appm/fpy for the He production.

TABLE II

NUCLEAR HEATING DENSITY (W/cm^3) IN IN-PORT CASSETTE COMPONENTS (NUMBERING REFERS TO FIG. 9)

#	Component	Maximum Nuclear Heating density (W/cm^3)	Position
1	In-Port RNC Collimators - Tubes	1.92×10^{-2}	LoS 26
2	In-Port RNC Collimators - Supports	2.47×10^{-2}	LoS 26
3	Cassette Structure	1.89×10^{-3}	
4	Cassette Electrical Feedthroughs	4.23×10^{-6}	
5	Cassette SVS Feedthrough	3.24×10^{-5}	
6	Cassette Supports to DSM	1.26×10^{-4}	
7	Fission Chamber housing	8.60×10^{-5}	LoS 1
8	Single Crystal Diamond Matrix Housing	5.10×10^{-5}	LoS 1
9	Collimator tubes Inside Cassette	1.40×10^{-4}	LoS 1
10	B_4C Shielding	3.64×10^{-3}	
11	Beam Dumps	6.57×10^{-5}	

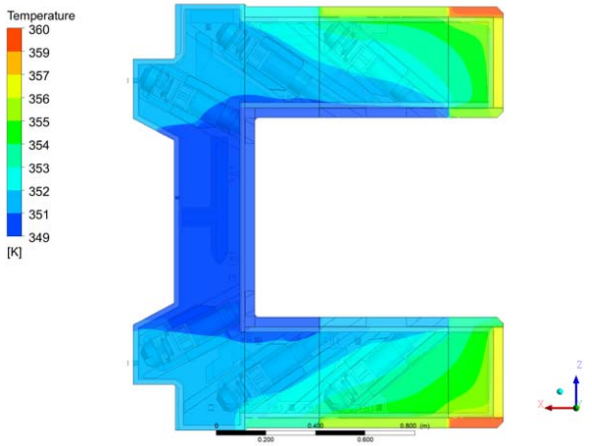

Fig. 10. Temperatures obtained through the thermal analysis performed using nuclear heat loads inputs.

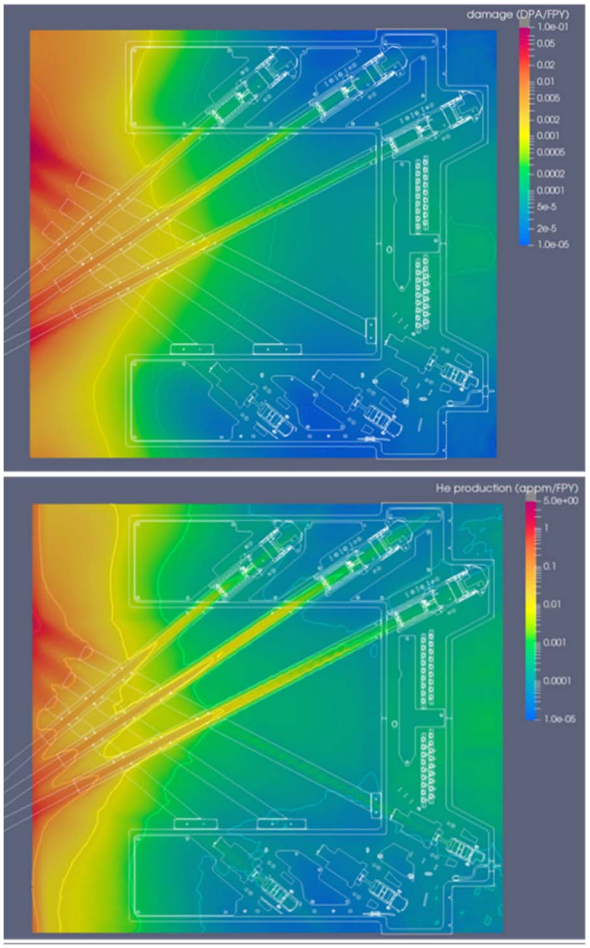

Fig. 11. Sections of the damage (dpa/FPY, top panel) and He production (appm/FPY, bottom panel) maps on stainless steel across the upper LoS.

A dedicated analysis has been performed to analyze the effect of radiation on ceramic components: insulation rings of FC and sCD detectors and insulators within the electrical feedthrough. These components are made of polycrystalline alumina (Al_2O_3) which is relatively resistant to damage with respect to other oxides. According to [18], the Al_2O_3 swelling characteristics do not increase by more than 20% for damage up to 20 dpa; moreover, the damage dose required to produce a degradation such that the alumina can no longer be regarded as a good insulator is $\sim 10^{-3}$ dpa. The cumulative damage (integrated over 2×10^7 s ITER lifetime) for the FC and sCD detectors and electrical feedthrough insulators is 6.34×10^{-5}, 1.65×10^{-5}, and 6.08×10^{-5} dpa, respectively, values well below the recommended threshold.

IV. NEUTRON SPECTRA FOR MEASUREMENT PERFORMANCE ASSESSMENT

The determination of the spectra at the detector's position for each in-port LoS has been made using a neutron source provided to the MCNP code through an external file defining a toroidally invariant neutron emissivity source mapped on a 40×40 matrix: it derives from a 15-MA peaked density DT ITER scenario and takes into account the Doppler broadening of the neutron spectra due to the variation of the ion temperature along the plasma profile. The calculation of the neutron spectra has been performed using standard F5 tallies (point detectors) in order to obtain the breakdown into the direct (uncollided) and scattered (collided) components. The expected neutron spectra at the detectors are shown in Fig. 12, where the breakdown into the direct and scattered components are reported for upper LoS FC and sCD, respectively.

The scoring positions have been placed in the middle of the sensitive area of the FC and at the position of the central pixel of each sCD matrix. The collided component presents some statistical fluctuations especially in the energy range 10–13 MeV mainly due to the fact that the spectra have been computed using a very fine energy binning (100-keV bins from 0 up to 10 MeV and 50-keV bins from 10 MeV onward) in order to be properly folded with the detectors response functions [3]. This operation allows the generation of synthetic data that can be verified in terms of compliance with the ITER measurement requirements for the neutron emissivity profile reconstruction [5].

Table III summarizes the results of the measurement performance analyses: for each LoS, the breakdown of the spectra into the collided and uncollided components is reported for

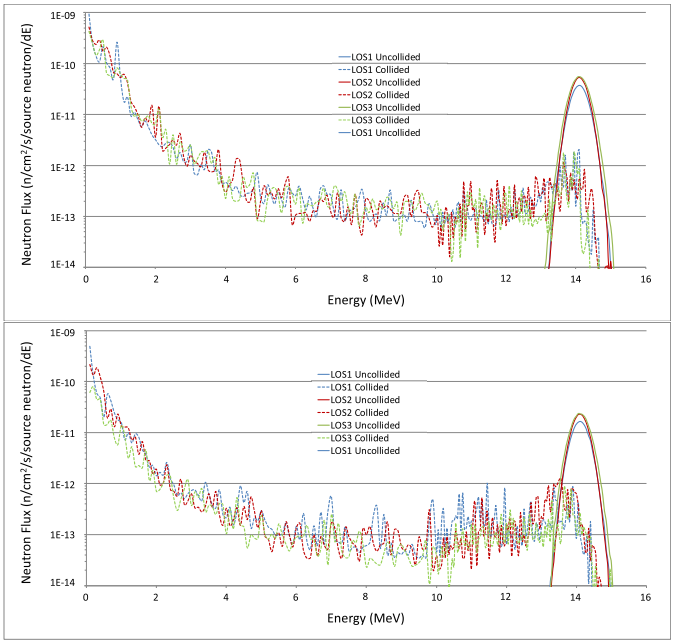

Fig. 12. Neutron spectra for the upper LoS detectors: FC (upper plot) and sCD (lower plot).

TABLE III

DIRECT (UNCOLLIDED) AND SCATTERED (COLLIDED) NEUTRON FLUX AT THE DETECTOR'S POSITIONS. THE UNCOLLIDED/COLLIDED RATIOS FOR EACH LOS ARE ALSO REPORTED

Detector	LOS	Uncollided Neutron Flux (n/sec/cm²)	Collided Neutron Flux (n/sec/cm²)	Uncollided/ Collided
Fission Chamber	1	3.72×10⁹	4.28×10¹⁰	0.087
	2	4.97×10⁹	4.21×10¹⁰	0.118
	3	5.84×10⁹	3.41×10¹⁰	0.171
	26	3.36×10⁹	7.59×10¹⁰	0.044
	25	4.07×10⁹	4.33×10¹⁰	0.094
	24	5.06×10⁹	4.23×10¹⁰	0.120
sCD matrix	1	1.63×10⁹	1.80×10¹⁰	0.091
	2	2.18×10⁹	1.66×10¹⁰	0.131
	3	2.53×10⁹	1.30×10¹⁰	0.194
	26	1.45×10⁹	2.63×10¹⁰	0.055
	25	1.64×10⁹	1.43×10¹⁰	0.115
	24	2.46×10⁹	1.45×10¹⁰	0.169

both FC and sCD detectors. The neutron flux values have been normalized to the 1.83×10^{20} s^{-1} neutron rate.

The uncollided/collided ratio highlights that the detectors closer to the DFW (i.e., LoS 1 and LoS 26) present a significantly higher neutron background level since they look at the plasma edge. Indeed, the components of the collided neutrons can be summarized as follows.

1) Neutrons scattered in the port plug and detector cassette (scattering): neutrons reach the detectors after having had their last interaction, respectively, in the port plug or the detector cassette.
2) Neutrons scattered in the collimators (in-scattering): neutrons coming from the plasma region defined by the collimator that enters the collimator and suffers few scatterings before reaching the detectors.
3) Backscattered neutrons (backscattering): neutrons scattered from the inner vessel region opposite any RNC LoS that enter the collimator. The backscattering therefore only depends on the position of the LoS, being more relevant for edge LoS.

The scattering component is negligible (Fig. 13).

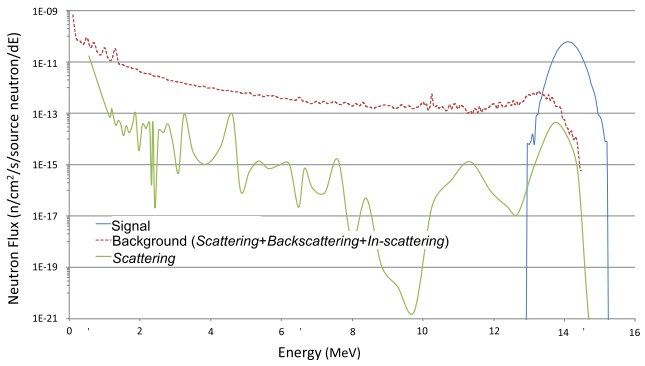

Fig. 13. Signal and background components in in-port detectors (LoS 3).

The calculated neutron spectra have been used as input for the measurement performance analysis through the Measurement Software Simulation Tool (MSST [4]) code that generates synthetic data representing the expected line-integrated flux measurement (brightness) and reconstructs the associated neutron emissivity profile through the spatial inversion of the simulated measurement. The results of this analysis [4] show that the actual RNC design satisfies the ITER neutron emissivity measurement requirements for the considered plasma scenario: $10^{14} - 4 \times 10^{18}$ neutrons $m^{-2} \cdot s^{-1}$ with 10% accuracy, 1-ms time resolution, and $a/10$ space resolution (a = minor radius).

V. CONCLUSION

An updated nuclear analysis has been performed for the ITER RNC in-port subsystem.

The neutrons/photons flux spatial distribution and nuclear heating density have been provided by means of detailed maps, with statistical uncertainty on each voxel <10% in the area of interest.

The assessment of the nuclear heat density on all the in-port RNC subcomponents has been carried out taking into account both the contribution from neutrons and secondary gammas as well as the impact of the crosstalk effect from the other diagnostic systems integrated into the EP01.

Thermal and thermomechanical analyses for the ITER normal operation conditions have been performed using as input the nuclear heat load calculated on all in-port RNC components as well as the thermal loads due to direct contact and thermal radiation with the DSM. The results show that the maximum temperature reached by the detectors is well below their operational limits.

The neutron spectra at the detector's position have been determined for the sCD matrix and FC in each in-port LoS,

with the breakdown into the direct (uncollided) and scattered (collided) components. The reconstruction of the neutron emissivity profile for the given plasma scenario, carried out by means of the MSST code, highlighted that the present in-port RNC layout is able to satisfy the ITER measurement requirements in terms of accuracy and time/space resolution.

ACKNOWLEDGMENT

The computing resources and the related technical support used for this work have been provided by CRESCO/ENEAGRID High Performance Computing infrastructure and its staff [19]. F4E: This article reflects only the views of the authors, Fusion for Energy cannot be held responsible for any use of the information contained therein. ITER: The views and opinions expressed herein do not necessarily reflect those of the ITER Organization.

REFERENCES

[1] D. Marocco, B. Esposito, and F. Moro, "Neutron measurements in ITER using the radial neutron camera," *J. Instrum.*, vol. 7, no. 3, Mar. 2012, Art. no. C03033.

[2] M. Cecconello, S. Conroy, D. Marocco, F. Moro, and B. Esposito, "Neural network implementation for ITER neutron emissivity profile recognition," *Fusion Eng. Des.*, vol. 123, pp. 637–640, Nov. 2017.

[3] D. Marocco, B. Esposito, and F. Moro, "Combined unfolding and spatial inversion of neutron camera measurements for ion temperature profile determination in ITER," *Nucl. Fusion*, vol. 51, no. 5, May 2011, Art. no. 053011.

[4] B. Esposito *et al.*, "Progress of design and development for the ITER radial neutron camera," *J. Fusion Energy*, 2022.

[5] D. Marocco *et al.*, "System level design and performances of the ITER radial neutron camera," in *Proc. 26th IAEA Fusion Energy Conf.*, Kyoto, Japan, 2016, pp. 1–8.

[6] D. Rigamonti *et al.*, "Neutron spectroscopy measurements of 14 MeV neutrons at unprecedented energy resolution and implications for deuterium–tritium fusion plasma diagnostics," *Meas. Sci. Technol.*, vol. 29, no. 4, Apr. 2018, Art. no. 045502.

[7] M. Cecconello *et al.*, "Strategy and guidelines for the calibration of the ITER radial neutron camera," *Fusion Eng. Des.*, vol. 146, pp. 2049–2052, Sep. 2019.

[8] F. Moro *et al.*, "The ITER radial neutron camera in-port system: Nuclear analyses in support of its design development," *Fusion Eng. Des.*, vol. 146, pp. 236–241, Sep. 2019.

[9] "X-5 Monte Carlo team: MCNP—A general Monte Carlo N-particle transport code, version 5," LANL, Santa Fe, NM, USA, Tech. Rep. LACP-03-0245, 2005.

[10] Y. Wu and FDS Team, "CAD-based interface programs for fusion neutron transport simulation," *Fusion Eng. Des.*, vol. 84, pp. 1987–1992, Jun. 2009.

[11] D. Leichtle *et al.*, "The ITER tokamak neutronics reference model C-model," *Fusion Eng. Des.*, vol. 136, pp. 742–746, Nov. 2018.

[12] V. S. Udintsev *et al.*, "Final design of the generic equatorial port plug structure for ITER diagnostic systems," *Fusion Eng. Design*, vols. 96–97, pp. 993–997, Oct. 2015.

[13] (2018). *FENDL-3.1d: Fusion Evaluated Nuclear Data Library Versions 3.1d.* [Online]. Available: https://www-nds.iaea.org/fendl/

[14] S. W. Mosher *et al.*, *ADVANTG—An Automated Variance Reduction Parameter Generator*, document, Rec. ORNL/TM-2013/416, 2013.

[15] A. Serikov *et al.*, "Neutronic analysis for the edge charge exchange recombination spectroscopy in equatorial port of ITER," *Fusion Eng. Des.*, vol. 165, Apr. 2021, Art. no. 112256.

[16] R. Kantor *et al.*, "Thermo-hydraulic modeling of the ITER radial neutron camera," *AIP Conf.*, vol. 2239, no. 1, 2019, Art. no. 020021.

[17] M. J. Norgett, M. T. Robinson, and I. M. Torrens, "A proposed method of calculating displacement dose rates," *Nucl. Eng. Des.*, vol. 33, no. 1, pp. 50–54, Aug. 1975.

[18] G. P. Pells and M. J. Murphy, "The effects of transmutation products on the radiation-induced swelling of Al_2O_3 and $MgAl_2O_4$," *J. Nucl. Mater.*, vol. 183, no. 3, pp. 137–144, Aug. 1991.

[19] F. Iannone *et al.*, "CRESCO ENEA HPC clusters: A working example of a multifabric GPFS spectrum scale layout," in *Proc. Int. Conf. High Perform. Comput. Simulation (HPCS)*, Dublin, Ireland, Jul. 2019, pp. 1051–1052, doi: 10.1109/HPCS48598.2019.9188135.